Effects of Local Coulomb Potentials on Acid and Base Protonation–Deprotonation Rates and Equilibria

SYLWIA SMUCZYŃSKA, JACK SIMONS

Chemistry Department and Henry Eyring Center for Theoretical Chemistry, University of Utah, Salt Lake City, UT 84112

Received 2 December 2008; accepted 27 February 2009
Published online 30 April 2009 in Wiley InterScience (www.interscience.wiley.com).
DOI 10.1002/qua.22230

ABSTRACT: Ab initio electronic structure methods, even when performed at a very modest level, applied to the energy profiles for deprotonation of an organic acid or of a protonated amine in the presence of proximal charged groups yield data that suggest the following: 1. The proton affinity of an amine tethered to a surface can be altered substantially by the presence of proximal positively charged groups. 2. Barriers (above the thermodynamic energy requirement) along the amine protonation–deprotonation pathway arise when positive charges are tethered nearby. 3. A competition between the attractive intrinsic N—H bonding potential and the repulsive Coulomb potential between the departing proton and the proximal positive charges is the primary source of the above two results. 4. There is much less change in the equilibrium constant K or the deprotonation and protonation rate constants k_1 and k_{-1} for an organic acid tethered to a surface when in the presence of proximal negative charges. 5. The attractive intrinsic O—H bonding potential and the attractive Coulomb potential between the proton and the proximal and nascent negative charges act in concert in the organic acid case. So, unlike the amine example, there is no competition between the dominant potentials and, as a result, no pronounced barriers occur along the reaction path. The relevance of these findings to acid–base properties of surfaces and nanoparticles are discussed. Int J Quantum Chem 109: 3120–3130, 2009

Key words: Coulomb potential; acid–base; proton affinity

Correspondence to: J. Simons; e-mail: simons@chem.utah.edu
Sylwia Smuczyńska is on leave from the Department of Chemistry, University of Gdansk, Gdansk, Poland.
Contract grant sponsor: National Science Foundation.
Contract grant number: CHE 0806160.

1. Introduction

In this article, we consider the effects of proximal charged groups' Coulomb potentials on the equilibrium constants K and dissociation k_1 and recombination k_{-1} rate constants associated with base

$$R - NH_3^+ \underset{k_{-1}}{\overset{k_1}{\rightleftharpoons}} R - NH_2 + H^+ \qquad (1)$$

and organic acid

$$R - COOH \underset{k_{-1}}{\overset{k_1}{\rightleftharpoons}} R - COO^- + H^+ \qquad (2)$$

deprotonation. This work is aimed at providing insight into how these rate and equilibrium constants might be altered if the amine or organic acid is tethered to the surface of, for example, an aerosol particle and in close proximity to other tethered amine or acid groups some of which are charged. Before detailing the methods used and presenting our results, let us illustrate the potential relevance of the kind of information obtained here with an example from surface science.

The study of the dissociation equilibria of surface-bound functional groups having acidic or basic character has received considerable recent attention (see e.g., [1]). For example, silica and silicate glass surfaces (A nice overview is given for these systems in Ref. 2) placed in water acquire a negative surface charge density through the dissociation of surface-bound silanol groups R-SiOH, and the degree of dissociation depends on an equilibrium involving counter ions (including H^+) at the surface and free ions in the bulk liquid in contact with the surface. In this example, the degree of dissociation as follows:

$$R\text{-}SiOH \rightarrow R\text{-}SiO^- + H^+ \qquad (3)$$

is governed by an equilibrium condition,

$$\frac{[H^+]_s[R - SiO^-]}{[R - SiOH]} = K(\text{moles/l}) \qquad (4)$$

where $[H^+]_s$ is the concentration of H^+ ions near the surface and [R-SiO$^-$] and [R-SiOH] are the concentrations (moles per unit area) of charged and uncharged silanol sites on the surface. However, $[H^+]_s$ is not the bulk concentration of H^+ ions but is the concentration in the liquid close to the silanol surface. A second equilibrium condition as follows:

$$[H^+]_s = [H^+]_{bulk}\exp(-\beta e\psi_s) \qquad (5)$$

must be used to determine the H^+ concentration at the surface in terms of $[H^+]_{bulk}$, the H^+ concentration in the bulk liquid. Here, β is $1/kT$, e is the unit of charge, and ψ_s is the electrostatic potential at the surface. As discussed in Ref. 2, the determination of the electrostatic potential at the surface usually involves using a Poisson-Boltzmann model of the spatial distributions of the ions in the solution surrounding the surface. The use of such approximations to ψ_s, in turn, introduces a significant degree of uncertainty in the estimate of the surface concentration of H^+ ions and thus in the estimate of the surface concentration of R-SiO$^-$ charges. The density of negative charges on the surface [R-SiO$^-$] is subsequently determined, using Eq. (4) with the estimated ψ_s and an equilibrium constant K that is assumed to be independent of surface charging. As we show below, K may not independent of the concentration of nearby charges, so such investigations of surface-local concentrations should be modified to address this issue.

Of course, as noted earlier, acid–base dissociation equilibria involving species tethered to a surface arise in a wide variety of situations, for example, in aerosols, small water-solvated droplets, and other nanoscale particles that may be exposed to air or to a surrounding solution. Analogous situations occur in gas-phase ion-molecule reactions involving, for example, proton transfer from an acid HA to a multiply protonated macromolecule such as a peptide or small protein. In all of these cases, the effect of surface charging on the ability of any specific surface species to accept or donate a proton can also alter the associated K, k_1, and k_{-1} values as we illustrate in this article.

The present effort focuses on the effects of Coulomb potentials from proximal charged groups located on different molecules than the one undergoing deprotonation. Analogous effects arise, for example, when considering deprotonation of a poly-protic acid such as H_3PO_4, where the energy required to remove the first proton is considerably less than that required to deprotonate $H_2PO_4^-$ or HPO_4^{2-}. Such well-known textbook cases are distinct from what we are treating because here the proximal charges are located at different binding sites on the surface of a substrate.

In this work, we do not attempt to address the difficulties surrounding how one best solves for the electrostatic potential generated by the complex double-layer structure of ions surrounding a surface embedded within a liquid. Instead, we focus on the energy profiles (energy as a function of bond elongation) that govern the intrinsic (i.e., in the absence of surrounding solvent or counter ions) dissociation events arising in deprotonation of an organic acid [Eq. (2)] or of a protonated amine [Eq. (1)]. In particular, we consider such reactions for organic acids or amines tethered to a surface and spatially organized in a regular array determined by the location of the surface's binding sites available to the acid or amine molecules. The top two drawings in Figure 1 show the deprotonation reactions for amine and acid molecules under such conditions.

In Figure 1, the spatial pattern of the molecules bound to the surface is supposed to be representative, for example, of the distribution of molecules adsorbed to a solid surface or bound to the surface of a small aerosol or water droplet (In the latter two cases, we assume the radius of curvature of the particle is large enough to allow us to treat the local environment as nearly planar).

We carry out these reaction energy profile studies not only for an acid or protonated amine with no nearby charged groups (as in the top two drawings in Fig. 1) but also for cases in which the acid or protonated amine is surrounded by one or more charged groups chosen to model the local electrostatic environment induced by other acid molecules that have already been deprotonated or amines that are protonated. For example, the bottom two drawings in Figure 1 show the deprotonation reactions in which there are two nearby charged groups (positive in the amine example, negative in the carboxylic acid example). Because we treat only a single shell of surrounding charged groups, we must assume either (i) that other charged groups are much more distant or have been dielectrically screened sufficiently to ignore them or (ii) that our results should be interpreted in terms of the total Coulomb potential generated by whatever charged groups are close enough to be important.

The primary goals of these model studies are as follows:

i. to determine to what extent the presence of nearby charged groups alter the energy (ΔE) needed to effect the deprotonation (this relates to determining to what extent proximal charges can alter the equilibrium constant $K = k_1/k_{-1}$) and
ii. to see whether the combination of the intrinsic bond stretching potential and the electrostatic potentials arising from the surrounding charges generate barriers ($(E^{\ddagger})$) to bond cleavage above the thermodynamic endothermicity ΔE (these barriers would change k_1 and k_{-1}).

For example, when considering protonation of a surface-bound amine that is in close proximity to one or more already protonated amines, the energy profile is certainly expected to be repulsive at large nitrogen-proton distances. On the other hand, the profile will become attractive as the proton comes close to the nitrogen lone pair orbital and forms the new N—H bond. So, in such cases, we expect to observe a barrier in the overall energy profile.

The model systems used in this study are depicted in Figure 2. For the amine protonation simulation, we use methyl amine as our model compound; for the acid deprotonation case, we use acetic acid. Within a plane perpendicular to the model compound's C—N or C—C bond and containing the methyl group's carbon atom, we place 1, 2, 3, or 4 charges at a distance R from the methyl group's carbon. In Figure 2, we show the square, equilateral triangle, and linear geometries used to distribute these charges.

The square and triangular distributions were chosen to be representative of fourfold and threefold surface binding sites found in many surfaces; the simulations using two or one excess charge were carried out mainly for completeness. The range of R-values used (5, 10, 20, 30, 40, and 50 Å) was chosen to be representative of very sparse surface charging (R = 50 Å) to high-charging (R = 5 Å). To illustrate how these R-values relate to surface coverage, we note that the silanol sites on silica surfaces have a density [2] of about 8 sites/nm^2. Our smallest (R = 5 Å) fourfold site model has an area of 50 Å^2 and thus would (if the surface were similar in binding-site structure to silica and all sites were occupied) contain about four binding sites. In our R = 5 Å fourfold case, with charges at the four corners and another positive charge in its center, there are a total of two charges (the central charge plus 25% of each of the four peripheral charges), which corresponds to 50% surface coverage. In contrast, our R = 50 Å square model has an area of 4,900 Å^2 and thus a charge density of $2/(4{,}900\ \text{Å}^2) = 0.04/\text{nm}^2$ or 0.5% of the total site coverage. Thus, we believe the range of R-values

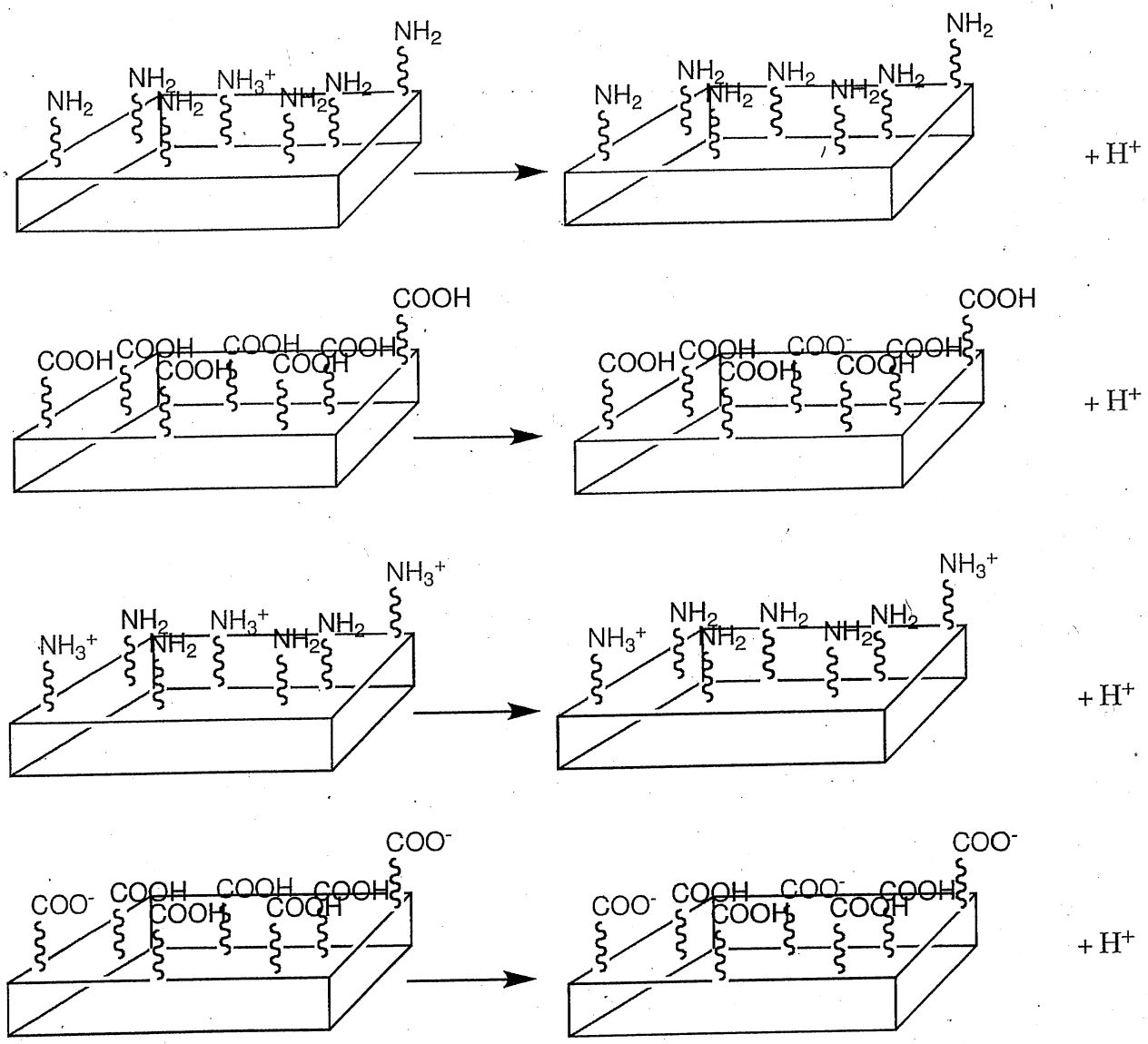

FIGURE 1. Deprotonation of a protonated amine (top) or of an organic acid (second from top) tethered to a surface surrounded by other amines or acids, none of which is charged. Deprotonation of a protonated amine (third) or of an organic acid (bottom) tethered to a surface surrounded by other amines or acids, two of which are charged.

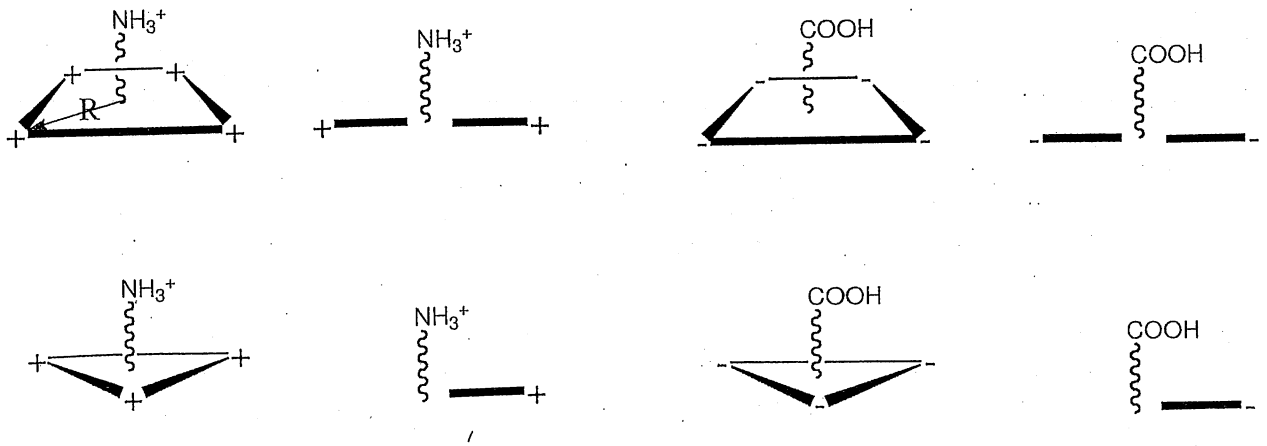

FIGURE 2. Four-, three-, two- and onefold distributions of charges surrounding the protonated amine or organic acid.

we employed allows us to draw conclusions pertinent to low- and high-coverage situations.

2. Methods

Our goal in this work was not to achieve highly accurate (i.e., ±1 kcal mol^{-1}) descriptions of the energy profiles for protonation and deprotonation of organic acids and bases. Rather, we wanted to focus on discovering and characterizing systematic trends and changes within these energy profiles caused by the presence of proximal charged groups. Therefore, essentially all of the calculations performed in this effort were carried out using straightforward Hartree–Fock (HF) self-consistent field (SCF) theory with only modest cc-pVDZ atomic orbital basis sets [3]. A few calculations were performed at the second-order Møller-Plesset (MP2) perturbation theory level to provide a comparison of HF, MP2, and experimental results and thus gauge the overall reliability of the results. We are able to make use of such low-level methods because the changes that the proximal charged groups give rise to are as follows: (i) larger than the energy improvements we could realize by using higher-level methods and (ii) straightforward to understand in terms of simple Coulomb energies in a manner that does not depend upon the level of theory we use.

For both the acetic acid and protonated methyl amine cases, the geometry of the parent compound (with no proximal charges) was first optimized at the HF level of theory. Subsequently, a series of geometries were generated in which the acid's O—H or one of the protonated amine's N—H bond lengths was increased (in small increments as shown later in plots). At each "stretched" bond length, the other (In the acetic acid case, we had to constrain the C—C bond length to be fixed at its value for the optimized geometry of the neutral. If we did not, the calculations converged, as we elongated the O—H bond length, to a state more relevant to H_3C^- and CO_2 and H^+, which is not the dissociation channel we wanted to follow) internal coordinates of the parent compound were relaxed to minimize the energy. As a result, we obtained the energy profiles for adiabatically deprotonating the O—H or N—H bond for these parent compounds. We note that, because these deprotonation steps involve heterolytic bond cleavage, it was appropriate to perform the calculations at the restricted Hartree–Fock (RHF) level as a result of which spin-contamination issues do not arise.

To obtain the energy profiles for deprotonation of the acid or protonated amine in the presence of proximal charges, we used the same series of geometries obtained when generating the reaction paths for the parent compounds and then carried out single-point RHF calculations with positive or negative charges located as described in Figure 2. To describe the peripheral positive charges, we placed H^+ cations (on which placed no basis functions to avoid having the peripheral sites' basis functions altering the description of the parent compound) at the locations shown in Figure 2. For peripheral negative charges, we placed F^- anions (with STO-3G basis functions [4]) at these locations. We used the same reaction-path geometries (i.e., those of the parent with no peripheral charges) to generate energy profiles when proximal charges are present because we wanted to focus only on the effects of the Coulomb potentials of these peripheral charges.

Finally, we note that all calculations were performed using the Gaussian 03 suite of programs [5].

3. Results and Discussion

In Figure 3, we display the energy profiles (The small "jumps" in the potentials near $r = 3$ Å for the cases with three and four proximal charges are artifacts. As one of the three N—H bonds is elongated, the departing proton (once the bond cleaves heterolytically) migrates in a manner that causes it to, for a limited range of r-values, approach one of the proximal positive charges. This close-approach, in turn, causes the potential to increase) obtained for six values of R and for 1, 2, 3, and 4 positive charges arranged as in Figure 2 for the protonation of methyl amine. On the vertical axis, the energy (relative to the energy of methyl amine at its equilibrium geometry) with no proximal charges is shown. On the horizontal axis, the length (r) of the N—H bond being elongated is given. Because of the very long range of the Coulomb potentials arising in these model compounds, we plot r on a logarithmic scale to allow us to display both the valence-range attractive portion of the potential and the asymptotic plateau behavior.

The trends that we glean from these energy profiles are as follows:

1. The minima are shifted to higher energy as the number of charges is increased (from 1 to

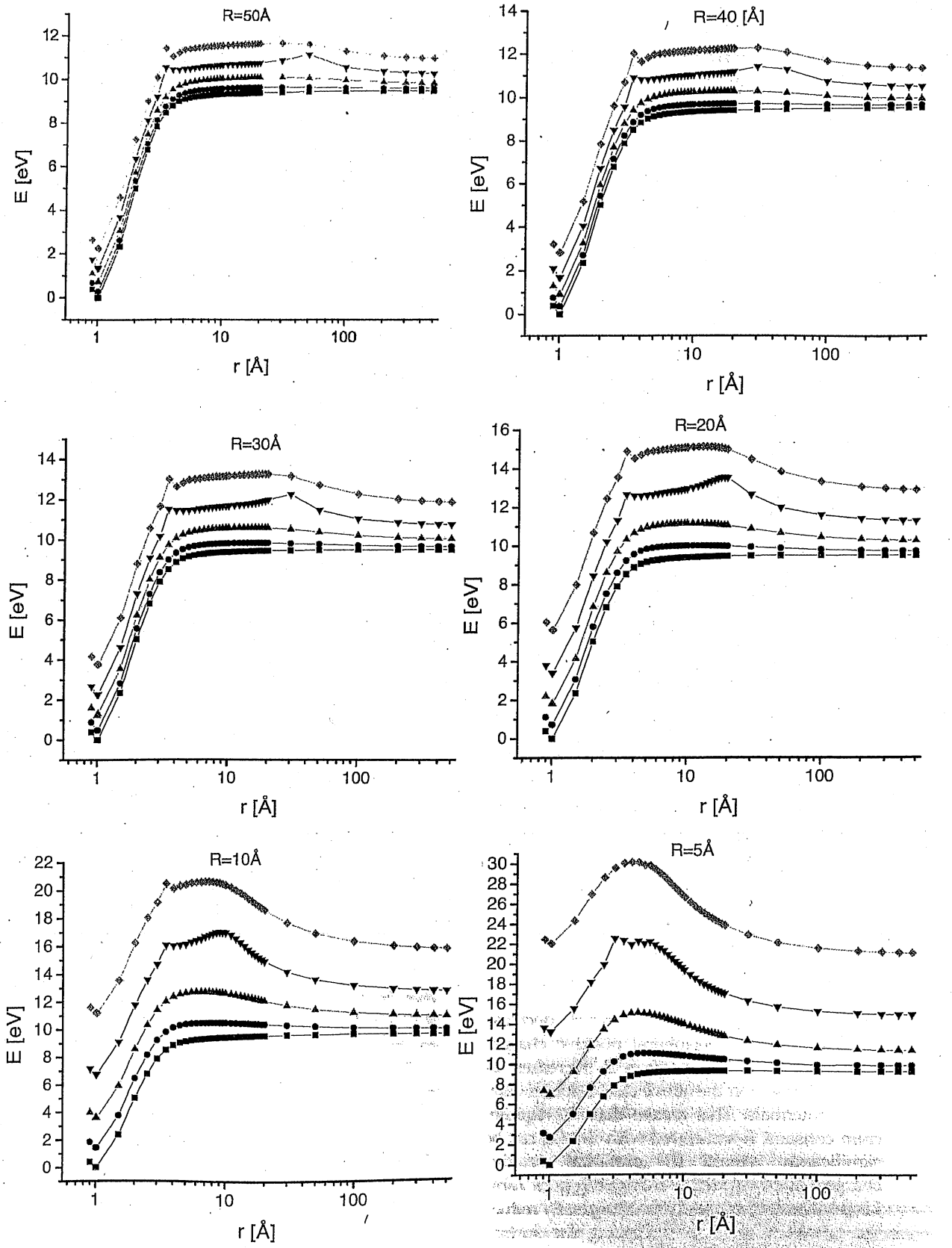

FIGURE 3. Energies as functions of the N—H bond length (r) of protonated methyl amine with zero (squares in each figure), one (circles), two (triangles), three (inverted triangles), and four (diamonds) positive charges located a distance R away from the methyl group's carbon atom as discussed earlier.

4) and as the distance (R) from the amine to the peripheral charges is decreased. It turns out that these energy shifts can be accounted for essentially fully in terms of the Coulomb repulsions ($V_{\text{periph.}}$) among the peripheral positive charges and the Coulomb repulsions (V) between the protonated amine and the peripheral charges.

2. The energies at the asymptotic plateaus are also shifted, and these shifts can be accounted for essentially fully in terms of the Coulomb repulsions ($V_{\text{periph.}}$) among the peripheral positive charges alone. It should be mentioned that the plateau energies shown in Figure 3 are those obtained at $r = 500$ Å. At this distance, the departing proton still experiences a (repulsive) Coulomb interaction from the underlying 1, 2, 3, or 4 positive charges. However, even when four peripheral charges are present and $R = 5$ Å, this residual Coulomb potential is only about 0.2 eV (To obtain more accurate values for the deprotonation energies in Table I, we could correct for these residual Coulomb energies. However, because they are so small, we chose to ignore them in this work). So, at the accuracy level appropriate to this study, we can ignore these small remaining Coulomb energies.
3. As a result of the Coulomb potentials discussed above, the deprotonation energies (the ΔE values for all cases are summarized in Table I) reflect a combination of two contributions as follows:

   a. the intrinsic heterolytic N—H bond dissociation energy (9.5 eV at the SCF level, 9.9 eV at the MP2 level, and 9.3 eV in experiment, as given in Table I),
   b. minus the Coulomb repulsion energy (V) between the central protonated amine and the peripheral charges that is lost once the proton has departed.

   The ΔE values shown in Table I clearly decrease as the number of peripheral positive charges increases and as the distance R decreases, as expected based on the above discussion of Coulomb potentials. This means that the equilibrium constant K associated with Eq. (1) can be significantly altered by proximal positive charges. Another point worth noting from Table I is that the data suggests one can greatly reduce the proton affinity by increasing the surface charge density and one may even be able to generate metastable species (i.e., with negative ΔE_r values) if one could achieve high-enough surface charging. At this time, it is not clear to us how one might achieve such high-coverage in practice, but we want to point this out for others to consider.

4. The energy profiles in Figure 3 also display barriers in excess of the bond cleavage energies. These barriers are most pronounced for small R-values but occur in all cases and can be quite large (i.e., much larger than kT at room temperature). Their existence suggests that the k and k_1 rate coefficients will be significantly different from what one would expect from the intrinsic N—H or O—H heterolytic dissociation energy profiles. In other words, the presence of proximal positive charges cannot only alter the equilibrium constant but can also affect these rates.

Let's now consider what is different between the case just studied in which a proton is removed from $H_3C—NH_3^+$ surrounded by 1, 2, 3, or 4 positive charges and the acetic acid case. One major difference that should be expected to have significant effects is that, for acetic acid, the proton experiences attractive forces from the intrinsic O—H bond potential and from the peripheral negative charges. In contrast, for the protonated methyl amine, the proton is attracted by the N—H bond potential but repelled by the peripheral positive charges.

In Figure 4, we display the energy profiles (These profiles do not suffer from the artifacts discussed earlier because elongation of the O—H bond does not cause the departing proton to come close to any of the proximal charges) obtained for five values [For $R = 5$ Å, we had difficulty converging the HF calculation because the strong Coulomb repulsions among the peripheral charges caused the F^- ions to become electronically unstable (i.e., to have positive energies for their highest occupied molecular orbital)] of R and for 1, 2, 3, and 4 negative charges arranged as in Figure 2 for the deprotonation of acetic acid.

The trends that we glean from these energy profiles are as follows:

1. The minima are shifted to higher energy as the number of charges is increased (from 1 to 4) and as the distance (R) from the amine to the peripheral charges is decreased. As in the methyl amine case, these energy shifts can be

TABLE I

Deprotonation energies (ΔE) and barriers ($E^{\ddagger}$) for deprotonation of protonated methylamine.

	Methylamine		
R (Å)	Number of charges	ΔE (eV)	($E^{\ddagger}$) (eV)
	0	9.50/9.88/9.3[a]	
50	1	9.31	9.42
	2	9.12	9.45
	3	8.93	9.86
	4	8.73	9.50
40	1	9.26	9.40
	2	9.02	9.43
	3	8.76	9.76
	4	8.50	9.50
30	1	9.17	9.36
	2	8.74	9.30
	3	8.48	10.00
	4	8.11	9.50
20	1	9.00	9.28
	2	8.46	9.34
	3	7.88	10.13
	4	7.26	9.48
10	1	8.46	9.03
	2	7.24	9.10
	3	5.88	10.15
	4	4.47	9.33
5	1	7.35	8.47
	2	4.62	8.28
	3	1.84	9.12
	4	-0.90	8.09

[a] Comparing the HF (9.5 eV) and MP2-level (9.9 eV) estimates of the proton affinity to the gas-phase experimental value (9.3 eV; This value is given in the NIST Chemistry WebBook [6]) gives some feeling for the overall accuracy of our energies.

accounted for essentially fully in terms of the Coulomb repulsions ($V_{periph.}$) among the peripheral negative charges. Unlike the amine case, here there are no Coulomb repulsions between the peripheral charges and the parent acetic acid prior to the acid's dissociation.

2. The energies at the asymptotic plateaus are also shifted, and these shifts can be accounted for essentially fully in terms of the Coulomb repulsions ($V_{periph.}$) among the peripheral positive charges and the Coulomb repulsion V between the nascent carboxylate anion and the peripheral charges. It should be mentioned that the plateau energies shown in Figure 4 are those obtained at r = 500 Å. At this distance, the departing proton still experiences an attractive Coulomb interaction from the underlying carboxylate ion and the 1, 2, 3, or 4 peripheral negative charges. However, even when four peripheral charges are present and R = 10 Å, this residual Coulomb potential is only about 0.3 eV (To obtain more accurate values for the deprotonation energies in Table I, we could correct for these residual Coulomb energies. However, because they are so small, we chose to ignore them in this work) so, again, they can be ignored.
3. As a result, the deprotonation energies (ΔE given in Table II) reflect a combination of two contributions as follows:
   a. the intrinsic heterolytic O—H bond dissociation energy (12.3 eV at the SCF level, 16 eV at the MP2 level, and 14.9 eV in experiment as given in Table II),
   b. plus the Coulomb repulsion energy (V) between the nascent carboxylate anion and the peripheral charges that is gained once the proton has departed.
4. Unlike the methyl amine case, we find very small, if any, barriers to deprotonation above and beyond the asymptotic energy requirements ΔE (Table II). For the amine, a competition between attraction (i.e., the intrinsic N—H bond potential) and repulsion (i.e., the Coulomb potential experienced by the departing H^+ due to the proximal positive charges) produced barriers. For acetic acid, both the intrinsic O—H bond potential and the Coulomb potential experienced by the departing H^+ due to the proximal and nascent negative charges are attractive, so no barriers occur.

4. Summary

Our primary findings are as follows:

1. The proton affinity of an amine tethered to a surface can be altered substantially by the presence of proximal positively charged groups.
2. Barriers (above the thermodynamic energy requirement) along the amine protonation–deprotonation pathway can also arise when positive charges are tethered nearby.
3. A competition between the attractive intrinsic N—H bonding potential and the repulsive

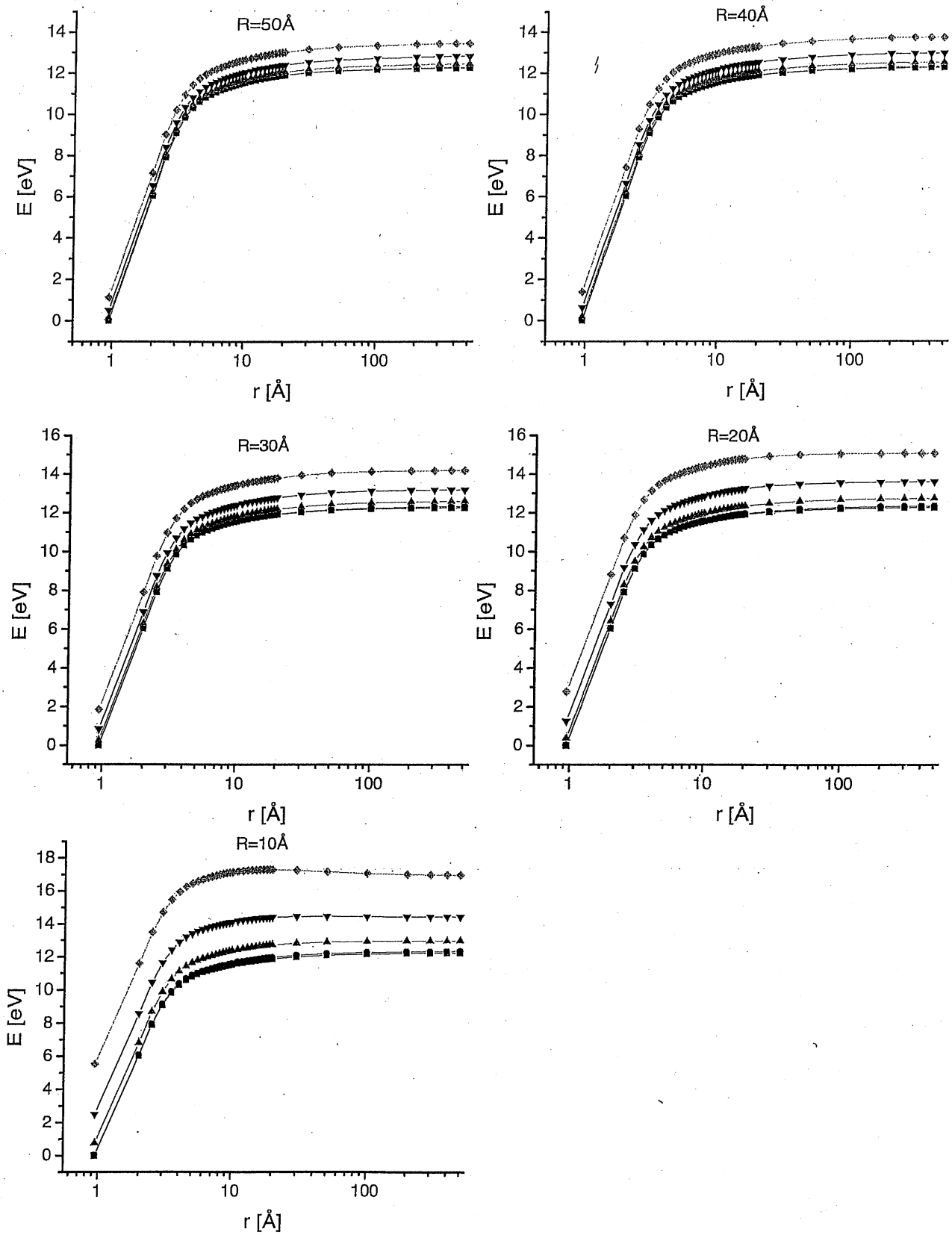

FIGURE 4. Energies as functions of the O—H bond length (r) of acetic acid with zero (squares in each figure), one (circles), two (triangles), three (inverted triangles), and four (diamonds) negative charges located a distance R away from the methyl group's carbon atom as discussed earlier.

TABLE II

Deprotonation energies (ΔE) and barriers ($E^{\ddagger}$) for deprotonation of acetic acid.

	Acetic acid		
R (Å)	Number of charges	ΔE (eV)	($E^{\ddagger}$) (eV)
	0	12.26/16.03/14.9[a]	
50	1	12.29	
	2	12.31	
	3	12.33	
	4	12.35	
40	1	12.30	
	2	12.33	
	3	12.34	
	4	12.35	
30	1	12.30	
	2	12.34	
	3	12.35	
	4	12.34	
20	1	12.32	
	2	12.35	
	3	12.32	
	4	12.25	
10	1	12.31	
	2	12.23	
	3	11.94	11.98
	4	11.45	11.79

[a] Comparing the HF (12.3 eV) and MP2-level (16.1 eV) estimates of the dissociation energy to the gas-phase experimental ΔH value (14.9 eV described earlier) gives some feeling for the overall accuracy of our energies.

Coulomb potential between the proton and the proximal positive charges is the primary source of the above two results.

4. There is much less change in the equilibrium constant K or the deprotonation and protonation rate constants k_1 and k_{-1} for an organic acid tethered to a surface when in the presence of proximal negative charges.
5. The attractive intrinsic O—H bonding potential and the attractive Coulomb potential between the proton and the proximal and nascent negative charges act in concert in the organic acid case. So, unlike the amine example, there is no competition between the dominant potentials and, as a result, no pronounced barriers occur along the reaction path.

Before closing, we should say a bit about influences that will act to "wash out" or qualitatively change the effects emphasized in this article. First, if the surface to which the acid or base molecules are tethered is immersed in water, the Coulomb potential between the dissociating proton and the surface positive (in the amine case) or negative (in the acid case) charges will be dielectrically screened for N—H or O—H distances beyond several Å. Moreover, the Coulomb interactions among the surface-bound charges will also be screened for R greater than several Å. In addition, if the surrounding water contains significant concentrations of other ions, Debye screening will act to cut off these Coulomb interactions (within the surface-bound species and between the departing proton and the surface charges) at the so-called Debye distance κ^{-1}, which depends on the ionic strength of the solution. For example, the Coulomb potential of a proximal surface charge 5, 20, or 50 Å distant will be screened out in a 1:1 electrolyte solution having concentrations 0.33, 10^{-2}, or 10^{-3} M, respectively.

Such strong solvation environments will therefore qualitatively change the nature of the energy profiles discussed above. To further illustrate, we note that the energy associated with deprotonating $H_3CNH_3^+$ in the gas phase is 9.3 eV as shown earlier. But the pK_a of $H_3CNH_3^+$ in aqueous solution at 298 K is 10.6 and the associated deprotonation enthalpy is only about 0.5 eV. The differential solvation energy (i.e., solvation of $H_3CNH_3^+$ vs. solvation of H_3CNH_3 and of H^+) clearly contributes much to this large change in deprotonation energy when comparing the gas-phase and aqueous environments. For acetic acid, the gas-phase energy associated with its deprotonation is 14.9 eV, whereas its aqueous (298 K) pK_a is 4.76 and the aqueous deprotonation enthalpy is −0.005 eV. In this case, the differential solvation energy effects are even larger because they involve differences between solvating neutral H_3C—COOH and solvating the two ions H_3C—COO^- and H^+.

The above discussion suggests that many of the features of the energy profiles shown in Figures 3 and 4 will be altered substantially for situations in which the surface to with the amine or acid molecules are tethered is immersed in water or in aqueous solutions of high-ionic strength. In contrast, for acids or amines tethered to surfaces of aerosols (i.e., with air surrounding them) or to nanoparticles suspended in solutions of low-dielectric constant and for gas-phase ion-molecule reactions, the screening and differential solvation effects discussed above will not act as strongly to overwhelm the influences of proximal

charged groups. Thus, it is probably in these latter such cases that the results provided in this article will be of most relevance.

ACKNOWLEDGMENTS

Significant computer time was provided by the Center for High Performance Computing at the University of Utah.

References

1. Borkovec, M., Jönsson, B.; Koper, G. J. M. In Surface and Colloidal Science; Matijevic, E., Ed.; Kluwer Academic/Plenum: New York, 2001; Vol. 16, p 99.
2. Behrens, S. H.; Grier, D. G. J Chem Phys 2001, 115, 6716.
3. Kendall, R. A.; Dunning, T. H., Jr.; Harrison, R. J. J Chem Phys 1992, 96, 6796
4. (a) Hehre, W. J.; Steart, R. F.; Pople, J. A. J Chem Phys 1969, 51, 2657; (b) Collins, J. B.; Schleyer, P. V. R.; Binkley, J. S.; Pople, J. A. J Chem Phys 1976, 64, 5142.
5. Frisch, M. J.; Trucks, G. W.; Schlegel, H. B.; Scuseria, G. E.; Robb, M. A.; Cheeseman J. R.; Montgomery, J. A., Jr.; Vreven, T.; Kudin, K. N.; Burant, J. C.; Millam, J. M.; Iyengar, S. S.; Tomasi, J.; Barone, V.; Mennucci, B.; Cossi, M.; Scalmani, G.; Rega, N.; Petersson, G. A.; Nakatsuji, H.; Hada, M.; Ehara, M.; Toyota, K.; Fukuda, R.; Hasegawa, J.; Ishida, M.; Nakajima, T.; Honda, Y.; Kitao, O.; Nakai, H.; Klene, M.; Li, X.; Knox, J. E.; Hratchian, H. P.; Cross, J. B. Adamo, C.; Jaramillo, J.; Gomperts, R.; Stratmann, R. E.; Yazyev, O.; Austin, A. J.; Cammi, R.; Pomelli, C.; Ochterski, J. W.; Ayala, P. Y.; Morokuma, K.; Voth, G. A.; Salvador, P.; Dannenberg, J. J.; Zakrzewski, V. G.; Dapprich, S.; Daniels, A. D.; Strain, M. C.; Farkas, O.; Malick, D. K.; Rabuck, A. D.; Raghavachari, K.; Foresman, J. B.; Ortiz, J. V. Cui, Q.; Baboul, A. G.; Clifford, S.; Cioslowski, J.; Stefanov, B. B.; Liu, G.; Liashenko, A.; Piskorz, P.; Komaromi, I.; Martin, R. L.; Fox, D. J.; Keith, T.; Al-Laham, M. A.; Peng, C. Y.; Nanayakkara, A.; Challacombe, M.; Gill, P. M. W.; Johnson, B.; Chen, W.; Wong, M. W.; Gonzalez, C.; Pople, J. A. Gaussian 03; Gaussian Inc.: Wallingford CT, 2004.
6. Available at: http://webbook.nist.gov/chemistry.